JOURNAL OF MATERIALS SCIENCE 9 (1974) 551–563

The development of ion-bombardment surface structures on stainless steel

M. J. WITCOMB
Electron Microscope Unit, University of the Witwatersrand, Johannesburg, South Africa

A brief review is given of the formation and characteristics of conical surface structures resulting from ion etching. The effect of low-energy ion bombardment of 18-8 stainless steel surfaces has been studied. The topography generated has been related to microstructural detail. The conical protrusions are found to arise from slag silicate particles while the pillar type structures result from fibrous manganese sulphide inclusions. Scanning electron microscopy has shown the development of both of these structure types to be in accord with previously published ion-etching models.

1. Introduction

Ion bombardment of solid surfaces generally does not result in uniform etching, but in the formation of surface structure. The characteristics of such topographical detail has been reported to be a function both of the state of the material and of the experimental conditions. The study of ion-etch structures to date has mainly been concerned with the introduction of foreign surface atoms or atom conglomerates and of the effect of surface contamination, oxidation, and polishing.

This paper reports an investigation of the effect of argon ion bombardment on the surface profile of 18-8 stainless steel. The cause and development of surface detail are investigated with respect to the specimen microstructure. Stainless steel has been chosen for examination since its expansion coefficient and oxygen resistance render it an ideal candidate for the substrate of superconducting a.c. power cables. During cable fabrication, a clean substrate surface would be imperative and ion bombardment could achieve the degree of cleanliness required. Since the condition of the substrate surface would be critical to the cables' performance, a knowledge of the surface state is essential. The paper begins with a brief review of previous work in which conical-type surface ion-etching structures have been observed. More general reviews of ion bombardment and sputtering are given in books by Kaminsky [1] and Carter and Colligon [2].

2. Conical ion-bombardment structures

The first observation of surface erosion by ion-bombardment processes was reported by Grove in 1852 [3]. Metallurgical interest in the technique then remained dormant for about a hundred years before it was found that for some purposes the method was superior to chemical etching [4, 5]. It is now known that, in general, there is a fairly close relationship between the selective etching at mechanical defects caused by chemical etching and that caused by ion beams [6, 7].

Fetz [8] was the first to discover a dependence of sputter yield on angle of incidence. One of the possible results of this observation, the formation of sub-microscopic surface cones, was reported in the same year, 1942, by Güntherschulze and Tollmein [9]. These authors noted that the cone phenomenon occurred on a wide variety of metals, the cone apex angle being different for each metal. Later, Spivak *et al* [10] described cone development at high current densities on ion-etched aluminium while Wehner [11] observed the formation of similar structures on silver (1 1 1) planes. Cone growth was attributed by these authors to migration of condensed metal atoms on the cathode surface.

The advent of the scanning electron microscope with its three-dimensional capability considerably enhanced research in the field of surface ion-bombardment effects. With this instrument, Stewart [12, 13], studying ion-etched (1 1 0) tungsten, showed that the surface conical

spikes could originate from either inclusions in the material or particles resting on the surface. Particles of low sputter yield were found to shield the higher yield material beneath them. When the shielding particle had been eroded away, a sharp spike or cone of matrix material remained. A similar behaviour has since been reported for iron oxide particles on iron [14], for etched NaCl [15], Al, Si, Sn [16], Au [17], InP [7] and stainless steel [18].

The shielding principle for cone formation has been substantiated by the work of Wehner and Hajicek [19]. They found that cones formed when groups of low sputter yield atoms, Mo or W, lay on the surface of high yield material such as Cu, Ag or Au. When the reverse yield combination occurred, however, such as Cu-Ag, no conical shapes were observed to develop. Papers by Thompson [20], Stewart and Thompson [16] have explained the etching rate in terms of a variation of sputter yield with the angle of incidence of the ion beam. As the surface is removed around the more slowly eroded particle, a structure forms so as to expose those faces having maximum sputter rate. This rate must be governed by the number of close-packed directions which intersect the surface since the process is believed to proceed via focused atomic collision sequences. Channelling patterns have been seen under low energy sputtering conditions by Wehner [21, 22] and at higher energies by Nelson and Thompson [23]. Since not all crystal directions result in equal atomic ejection, the rate will depend not only on the angle that each direction makes with the surface, but also the relative angle that each subtends to the ion beam [24]. Surface binding energy of the target atom would thus be expected to be an important factor since this varies with the crystal face involved. Cone faceting, a consequence of such a crystallographic dependence, has indeed been observed by Wilson and Kidd on bombarded gold [17].

Wehner and Hajicek [19] have noted the importance of solubility and activation energy for migration. For low yield carbon atoms seeded on a high yield Cu substrate, cones do not form under ion bombardment. When low yield Mo atoms replace the C atoms, conical structures form. The migration of Mo atoms not only forms a protecting surface nuclei, but acts as a replenishing process for the nuclei during actual bombardment. Such behaviour could explain the results of Güntherschulze and Tollmein [9]. Surface diffusion processes would be particularly enhanced by oblique ion bombardment or thermal agitation produced by heat generated from the ion-etch mechanism or an external heater. If diffusion were the dominant mechanism, surface-faceting of crystal planes with low free energy might then result. One would then expect an ion current density dependence [16], such as seen by Spivak *et al* [10].

Further investigations have elaborated on the development of surface structures. The conical protrusions have been found to always have their axes aligned along the direction of ion incidence, while the cone apex angle is reported to be directly related to the angle of ion incidence at which the sputter yield reaches its principal peak value [16]. The numerical value of the apex angle has been described in terms of ion-reflection effects [16, 25]. The conical structure has been shown not to be a steady state condition of the surface, since with continued ion etching the cone will diminish in size and finally disappear while maintaining its characteristic shape and apex angle throughout [26, 27]. A computer simulation of sputtered sinusoidal amorphous solid surfaces [28] predicts, in agreement with the theory of Barber *et al* [7], that a stable cone structure can only occur when the cone angle equals the angle of ion incidence for which the sputter yield is the same as for normal incidence. The computation indicates, however, that this only occurs after some 10 cm of surface had been etched away.

A schematic diagram of the formation of a surface cone has been published by Stewart and Thompson [16]. This has been indicated to be correct from studies on etched stainless steel [18]. More recently, Barber *et al* [7] have predicted shape development in good agreement with experimental observations using Frank's kinematic theory of crystal dissolution. Thornton [6] has highlighted the difficulty in shape development after fairly long bombardment times, of distinguishing between cones due to internal precipitates and those derived from surface contamination.

3. Experimental

The material studied in the present investigation was 18-8 stainless steel, type EN58J. The specimens were in the form of cylinders, each of which was 5.5 cm long, 2.3 cm i.d. and 0.1 cm thick. The inside surface of the cylinder was carefully machined to a mirror-like finish of

0.5 μm peak-to-peak roughness. It was this surface which was subject to bombardment by high purity argon ions. The cylindrical specimen and an axial niobium rod, diameter 0.3 cm, formed the electrodes of a self sustaining d.c. diode bombardment system.

With the specimen as cathode, ion bombardment was carried out at a pressure between 90 and 150 μm with ion energies of approximately 0.3 keV. Breakdown of the glow discharge occurred at 70 μm. The mean ion-current density on the specimen was regulated to average 600 μA cm^{-2}. This current yielded an etching rate of about 0.5 Å sec^{-1}. The ion-bombardment direction was effectively perpendicular to the specimen surface, a fact confirmed from a study of the ion-bombardment structures.

Thin foils of stainless steel were prepared for electron microscopy by electro-polishing in a 60% orthophosphoric, 40% sulphuric acid solution at 15 V, 1 A cm^{-2} followed by washing alternately in glacial acetic acid and hot methanol. All foils were subsequently viewed in transmission in a Siemens Elmiskop 1 Microscope operating at 100 keV. Unless stated otherwise, chemical etching of the specimen surface was carried out using a solution of 5 g ferric chloride, 50 ml hydrochloric acid and 100 ml water at 70°C. Chemically etched ion-bombarded surfaces and fracture surfaces were studied in a Cambridge S.4 Scanning Microscope. Precipitate analysis was performed on thin foils using an AEI EMMA-4 Analytical Microscope, and on fracture surfaces with a JEOL JXA-5A Electron Probe Microanalyser.

4. Results

4.1. Cone structures

Ion bombardment of the surface of 18-8 stainless steel did not cause any obvious contamination or discoloration of the surface such as observed for many materials by others [29, 30]. Initially, only increased surface roughness results. However, after about 1 h bombardment, which corresponds to a dose of 10^{19} ions cm^{-2}, a surface structure became discernible. This structure took the form of conical protrusions standing proud of the surrounding surface. Continued ion etching produced a rapid increase in the number of cones, Fig. 1. From an average of ten scanning micrographs per etching time, the relationship between the density of cones and ion-bombardment time is given in Fig. 2.

All the cone structures were seen to have their axes perpendicular to the specimen surface and, hence, parallel to the ion-beam direction. On average, the cone apex angle remained constant at 90°. Close inspection revealed that a large number of cones exhibited faceting to varying degrees. The facets tended to a hexagonal symmetry (Fig. 3). In general, a perfect hexagon was not achieved, only between two and four

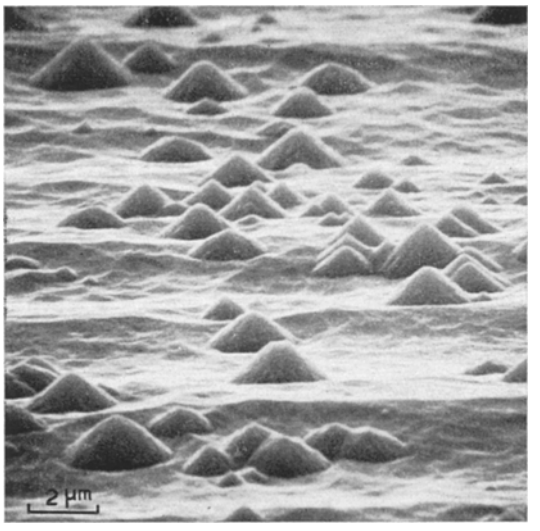

Figure 1 Cone shaped matrix protrusions on an ion-bombarded steel surface. Ion dose ~3 × 10^{20} 0.3 keV A^+ ions cm^{-2}.

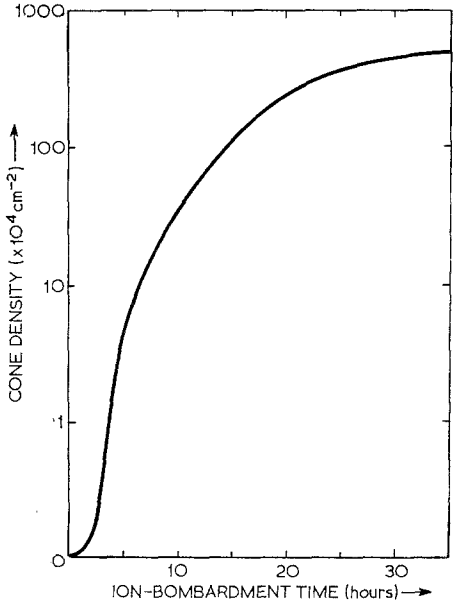

Figure 2 Graph of surface cone density on 18-8 steel versus ion-bombardment time.

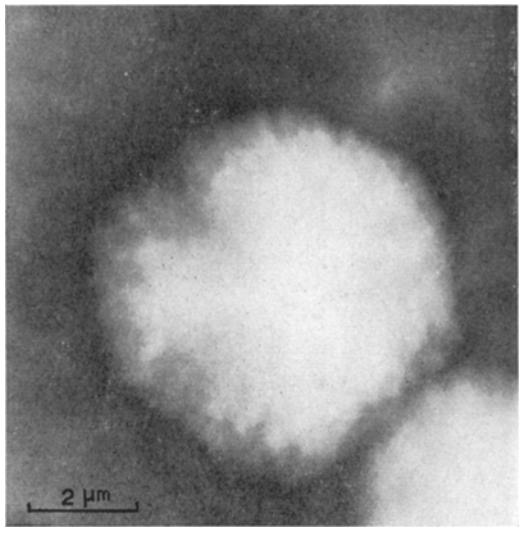

Figure 3 Hexagonal faceting on an ion-etched cone.

facets being recognizable on any one structure. Similar habit effects have been seen on argon etched gold [17] and probably result from the high sputter yield of low index crystal planes. The literature contains convincing evidence of ejections along ⟨100⟩, ⟨110⟩, ⟨111⟩, ⟨114⟩and ⟨116⟩ directions in fcc metals [31]. Hence, the above symmetry is easily possible together with other alternatives. The diameter of the faceted cones, in the present case, was always smaller than the matrix grain size and, hence, a single crystal effect.

Figure 4 A non-uniform arrangement of ion-bombarded cones. Clusters and rows of conical protrusions are in evidence.

A study of many ion-bombarded steel surfaces reveals the overall cone distribution to be fairly homogeneous. However, in particular after long bombardment times, some specimens exhibited a heterogeneous arrangement. Fig. 4 shows a typical example where the cones can be seen to cluster and lie in rows roughly parallel to the cylinder axis. Transmission electron microscopy negated a possible lattice defect-cone correlation since the samples were found to be virtually free of dislocation. In contrast, evidence of significant numbers of second phase particles about 1 μm in diameter was found. While some of these precipitates were positioned on grain boundaries, the majority were intergranular and not associated with any obvious nucleation site in the fcc austenite matrix (Fig. 5). Electron diffraction and elemental analysis on

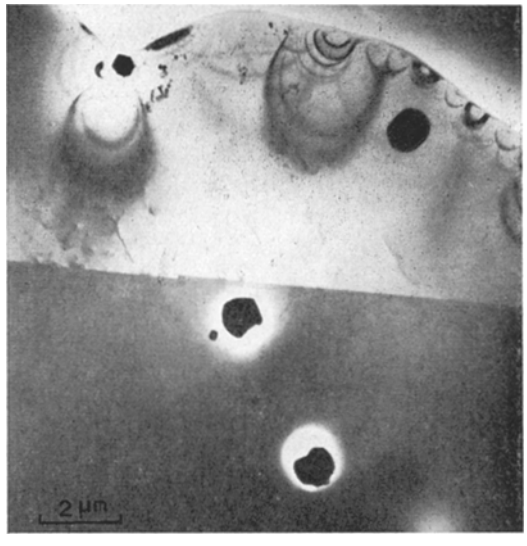

Figure 5 Transmission electron micrograph showing manganese silicate precipitates in a relatively defect-free austenitic matrix.

thin foils revealed these precipitates to be manganese silicate inclusions. They took the form of the orthorhombic phase Tephroite, Mn_2SiO_4 [32]. A composition range for the manganese silica components between Mn_3Si and Mn_5Si_3 was measured for the precipitates. Both manganese and silica are known to be deoxidizing additives for steel, the MnO also stabilizing the silicate in slag reactions [33].

To test for a possible relationship between these second phase particles and the conical surface structures, two methods were employed.

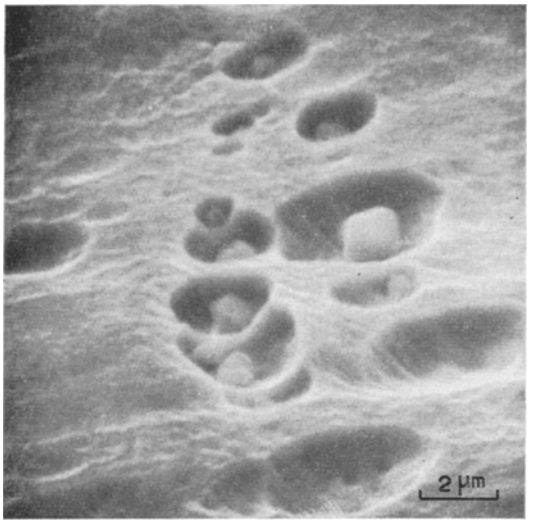

Figure 6 Scanning micrograph of a steel surface which has been lightly chemically etched. Rows of precipitates are shown to have been left proud of the surface.

In the first, steel surfaces were lightly chemically etched. Rows of precipitates were revealed (Fig. 6). These indicated that the cones shown in Fig. 4 could be derived from such nuclei. Secondly, fatigue fractures at room temperature induced by reverse plane bending were studied. Owing to specimen thickness, fractures were always made perpendicular to the specimen surface. Those perpendicular to the axial cylindrical direction will be termed transverse fracture, while those along the axial direction will be called longitudinal fractures. Transverse fractures (Fig. 7) show a large number of small precipitates. A few elongated particles are observable and these appear associated with channels running perpendicular to the fracture face. The significance of these particles will be discussed in the next section. Fig. 8 shows a longitudinal fracture

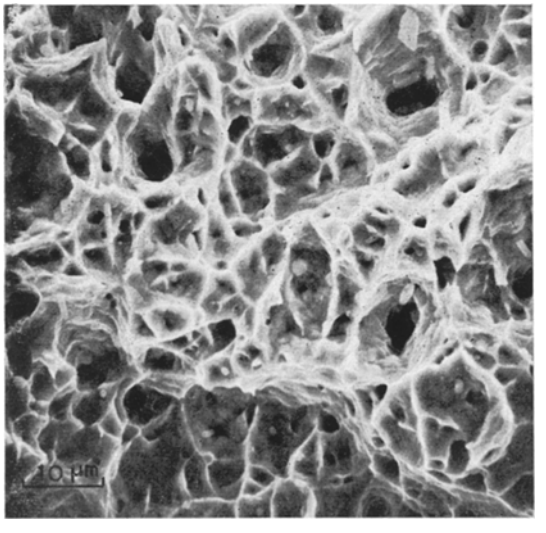

Figure 7 A transverse fracture showing precipitates and fracture channels perpendicular to the fracture face.

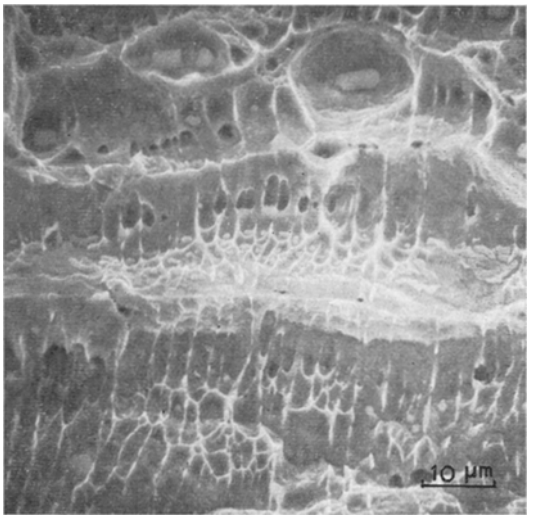

Figure 8 Longitudinal fracture surface revealing large numbers of slag silicate inclusions.

which has a ledge at the centre of view at right angles to the main fracture face. Such a fracture ledge is characteristic of a higher density of inclusions in a particular plane, and this serves to demonstrate the general overall presence of non-uniform particle distributions seen in this steel. Correspondence between precipitates and cones is evident and clearly indicates that precipitates were present in sufficient numbers to be possible cone nuclei. The vertical section of the face shows fewer precipitates as these are attached to the mate fracture surface. The small ledge precipitates were analysed as slag particles, calcium–aluminium–silicate of the type $CaO.Al_2O_3.2SiO_2$. Small amounts of other elements such as Cr and Mn were also present. Such inclusions were typically glassy in appearance, globular in shape and fluoresced under the electron beam.

If the cones are derived from lower sputter yield particles protecting a higher yield matrix then conclusive proof of a precipitate-cone correspondence might be possible to detect by careful study of the top of cones. As a first step, fracture surfaces were inspected to see if by

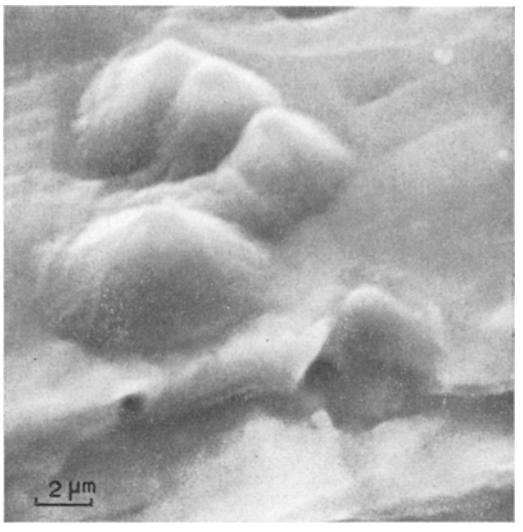

Figure 9 A fractured surface cone derived solely from precipitate material. The bottom half of the particle can be seen to have broken away from the conical top.

chance any cones had been positioned right across the fracture front. While the probability was small, a few cases were found of which Fig. 9 is an example. In this case, the top portion of a 2 μm elongated particle has been ion etched into a cone shape. Fracture of the specimen has caused the surface to cleave parallel to the surface such that this inclusion has fractured parallel to the surface. The lower part can be seen detached from its conical top. That an elongated particle can exist in this orientation is evidenced in Fig. 10. A later stage in the etching process was subsequently documented by quickly dipping a long-time bombarded specimen into hydrofluoric acid. This acid bath appeared very selective and conclusively revealed the existence of precipitates at the top of cones (Fig. 11). This figure illustrates the case for when the precipitate has been significantly etched away and the particle accounts for only the apex area of the cone structure.

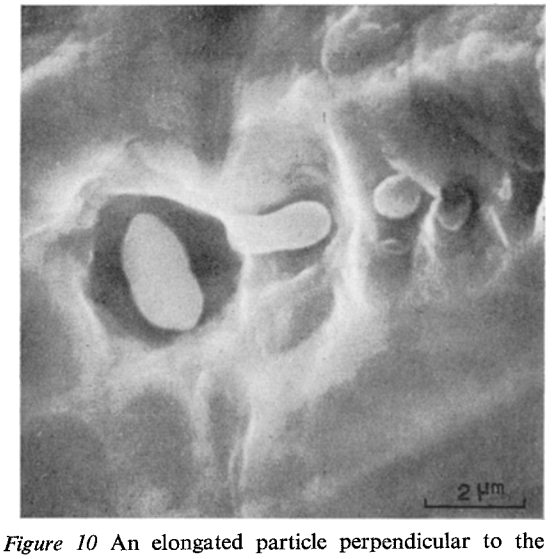

Figure 10 An elongated particle perpendicular to the specimen surface.

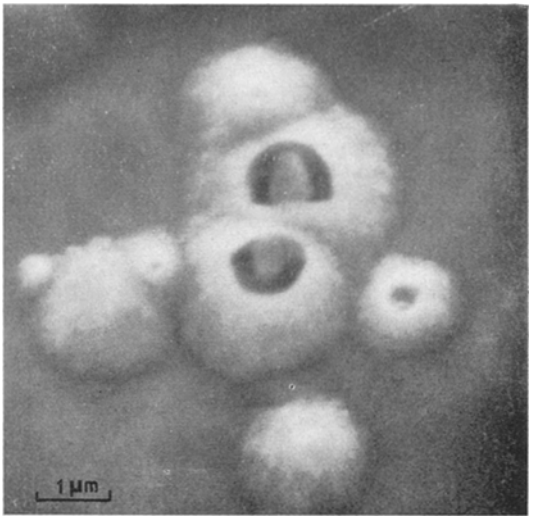

Figure 11 A scanning micrograph showing a manganese silicate precipitate at the top of a conical protrusion.

Stewart and Thompson [16] have proposed various stages in the formation of a conical ion-etching structure. The present investigation has indicated these to be essentially correct, the present observed topographical development process being summarized in Fig. 12. This figure includes an additional intermediate structure, the dome type structure (Fig. 12c) observed previously [18]. The cone type structure will almost always develop, since inclusions will always have at least an element of curved surface and this will contain a portion of high sputter yield orientation. This element will grow in preference to the lower yield slopes, the process having been predicted by others [7, 16, 26-28]. The configuration changes in Fig. 12 will apply to lower yield particles or contamination whether on or below the specimen surface. In the latter case, the overlying matrix material will have to be ion etched away first.

From Fig. 12 it can be seen that two sets of cones can develop. For large precipitates,

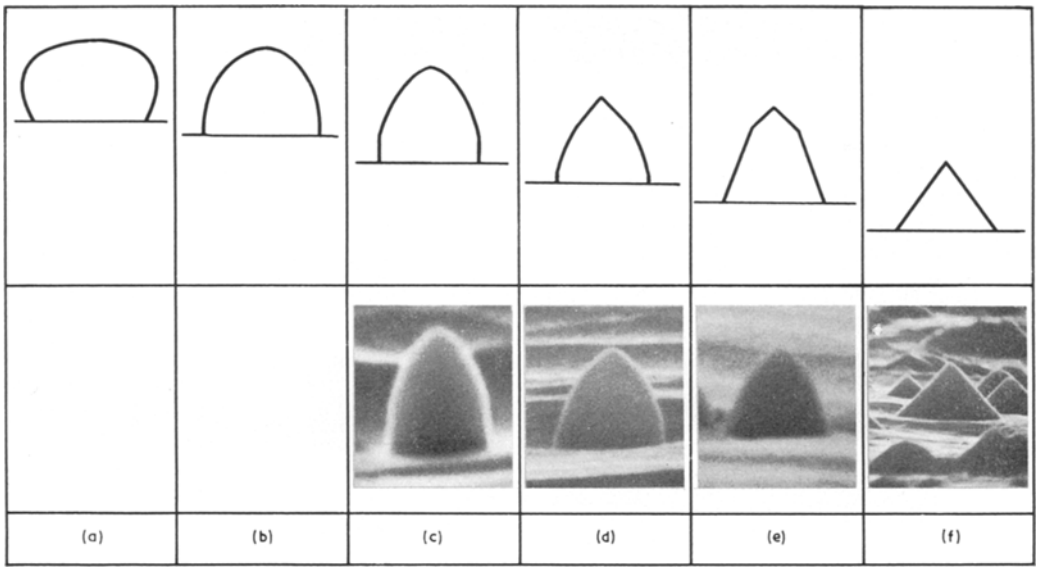

Figure 12 A schematic diagram of surface cone formation. Below are shown the corresponding scanning microscope structures.

inclusion cones are possible. Once the inclusion has been eroded away, matrix cones are formed. The latter case is illustrated in Fig. 1. Since the inclusion and matrix are of different composition, different shaped cones are expected. That is, the cone apex angle will be characteristic of the cone material. When the dimensions of the inclusion parallel to the specimen surface plane (x, y) are considerably greater than that in the z direction, the inclusion will be eroded away before the sides of the matrix protrusion meet to complete the characteristic conical shape. In such a case, a truncated cone results (Fig. 13). Further ion etching causes the sides to converge and finalize the cone. Of course, after long ion-bombardment times it is possible to see a good many of these structures on the same surface. This occurs because a range of inclusion sizes exists in the matrix and continued etching exposes fresh precipitates. An equilibrium condition arises under which cones are disappearing at the rate at which fresh precipitates are being uncovered. For steel specimens considered in the present study, this condition occurred after about 30 h bombardment.

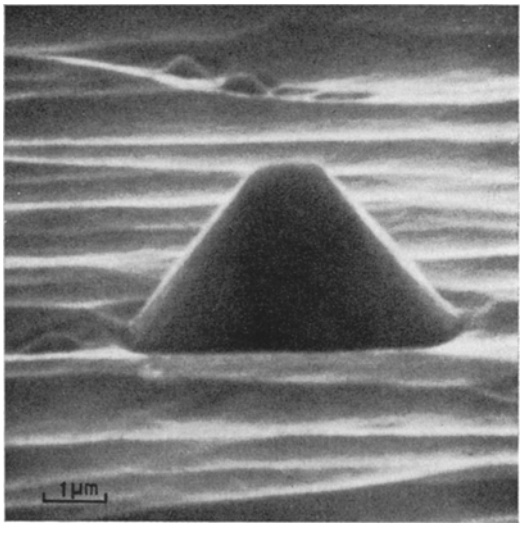

Figure 13 A matrix truncated cone left after the complete ion erosion of a plate-like precipitate.

It would not necessarily be expected that all cones originate from one precipitate. Clusters of two or three precipitates have been noted by transmission microscopy, and careful chemical etching of cones has shown such groups of precipitates to be present at the tops of cones (Fig. 14). When a cluster of second phase particles or a single dumb-bell shaped particle (see A in Fig. 15) is etched away from the cone apex, a characteristic complex jagged cone top results (Fig. 16). The effect of subsequent ion reflection and secondary sputtering often causes such a structure to develop into several separate cones. For the case of one precipitate above another, the shape in Fig. 17 can evolve. In this case, the top particle was the smaller of the two.

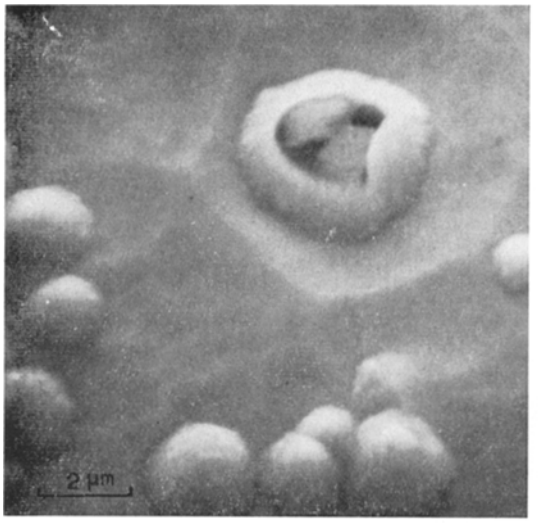

Figure 14 A cluster of Mn_2SiO_4 precipitates at the apex of a surface cone.

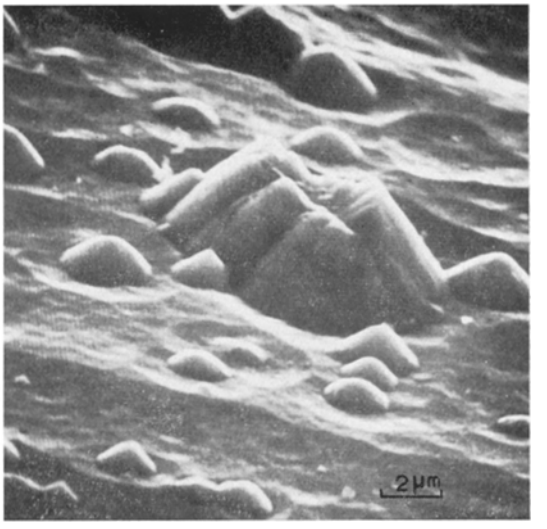

Figure 16 A complex jagged top to a cone after complete ion erosion of a cluster of precipitates.

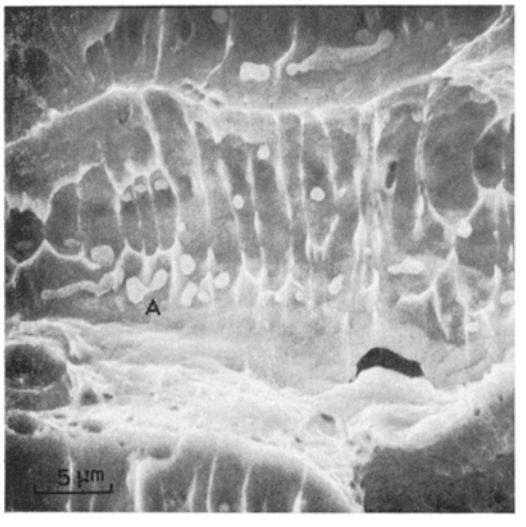

Figure 15 Longitudinal fracture revealing irregular globular type precipitates. A dumb-bell type inclusion can be seen at A.

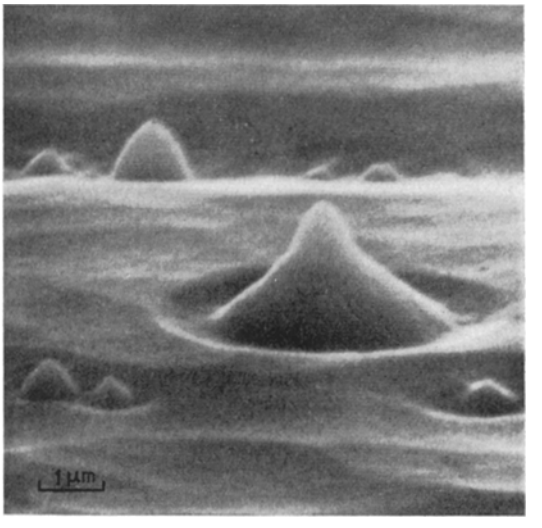

Figure 17 A structure resulting from two precipitates, the smaller being on top.

The crater surrounding the base of this structure is believed to arise from ion reflection [34].

4.2. Pillar structures

A second type of ion-bombardment structure has been observed on stainless steel. While this structure initially appears identical with the developing cones described in the previous section, close inspection reveals the structures to possess a greater secondary electron emission coefficient. A different composition is immediately indicated. Continued surface erosion yields a pillar or fibre type structure, Fig. 18. These pillars generally stand perpendicular to the surface and measure approximately 1 μm in diameter. The density of such features varies considerably across the surface. They may stand alone or in small clusters, Fig. 19.

A light chemical etch of the specimen surface, Fig. 20, has shown the pillars not to be any form of contamination or due to material sputtered

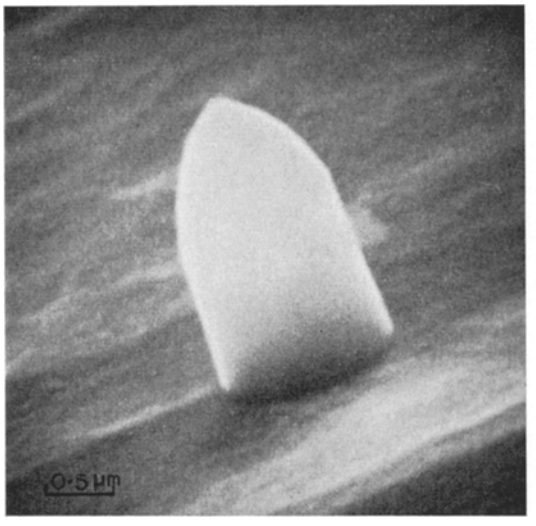

Figure 18 A pillar structure left standing proud of the steel surface after ion bombardment. Ion dose ~2 × 10^{20} 0.3 keV A^+ ions cm^{-2}.

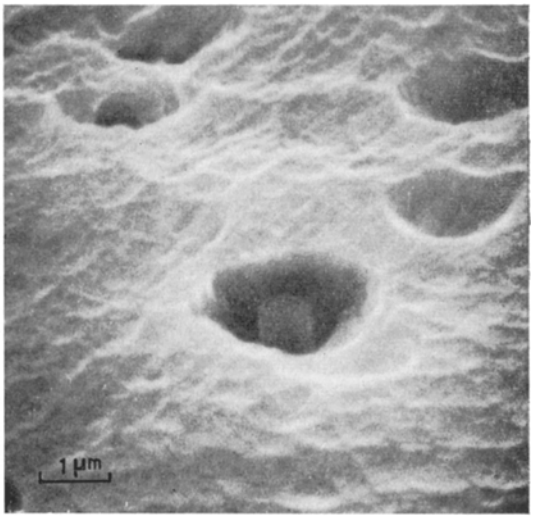

Figure 20 A chemical steel surface exhibiting a fibre structure in the matrix material. The flat end is a fracture face.

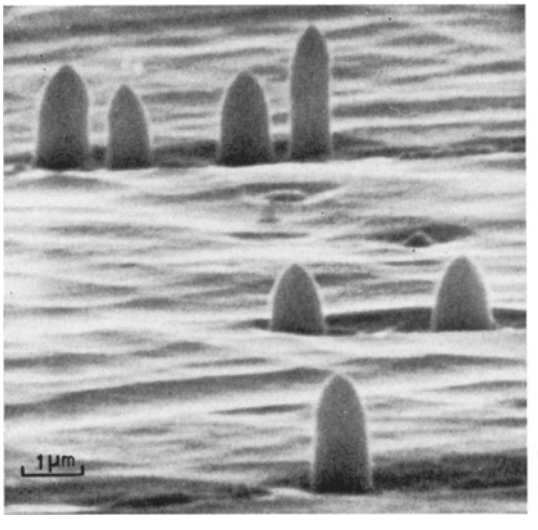

Figure 19 A small cluster of pillar surface structures.

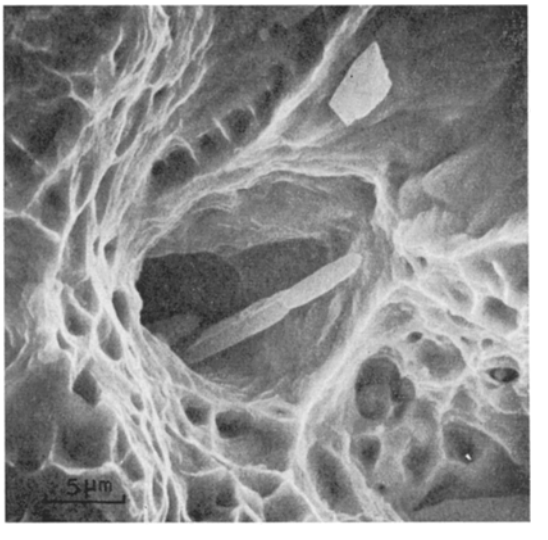

Figure 21 Longitudinal fracture surface showing a fibre structure protruding from a fracture channel.

from another part of the chamber, but to be part of the stainless steel microstructure. The flat end is probably a fracture face resulting from final sizing of the specimen by turning down the cylinder on a lathe. More typical is the rounded end shown in Fig. 21. The fibrous nature of the inclusion is clearly visible, the particle appearing to protrude from a fracture channel in the matrix material. This correlates with the transverse fracture surface seen in Fig. 7.

Ion bombardment of the fibres always results in the development of conical type ends of apex angle about 75°. As would be expected, the formation process of the fibre tip follows the same procedure as for the silicate precipitates. In general, however, dome type tips were seen to predominate. The general surface profile of the sides of the fibres and the angle that they make with the ion-beam direction determines the subsequent overall shape of the fibre protruding above the surface. This can be seen in Fig. 22.

Figure 22 A micrograph showing the effect of ion etching a bent pillar structure. The side to the ion beam has started to develop into the characteristic slope while the pillar tip has become conical in shape, and asymmetric.

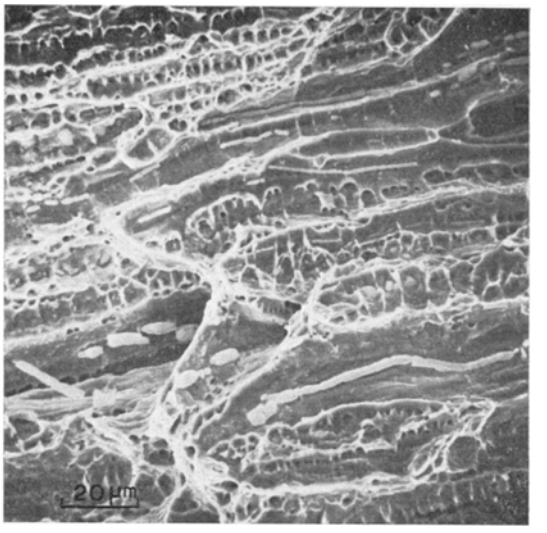

Figure 23 A longitudinal fracture face of steel exhibiting fibre structures parallel to the specimen axis.

Here a fibre makes an angle less than 90° with the surface. Considered from a two-dimensional point of view, one side is shielded from the etching beam while the other side changes to try to make an angle $90 - (\hat{\theta}/2)$ with the specimen surface. The pillar thus changes shape. Under such circumstances the conical tip, while still retaining its axis parallel to the ion beam, becomes asymmetric. It can thus be seen that final characterization of the etched pillar is markedly influenced by microstructural detail through the angle that the pillar subtends with the specimen surface. Owing to their relatively high strength, these structures do not appear to snap off after long bombardment as seen for NaCl [15].

Transmission electron microscopy of the pillars was not possible since their low density precluded their existence in any fabricated thin foil. Longitudinal fatigue fractures were utilized to study their characteristics in the bulk material. Such a study shows that by far the most fibres are parallel to the cylinder axis. The fibres vary in diameter from 1 to 3 μm, Fig. 23. The fracture surface can be seen to exhibit a channel dimple-like appearance. It might be expected that all elongated inclusions should be parallel to the cylinder axis due to the strains involved in steel tubing fabrication. However, the stress distributions occurring during the Mannesmann Mill type process are extremely complex. Some alignment off axis is possible as implied by the surface pillars and this has subsequently been confirmed from studies of many fracture faces. Fig. 24 is an example of fibres in the centre of the bulk showing alignment in the direction perpendicular to the surface. Such an occurrence is relatively rare and conforms to the low density of surface pillars.

Analysis of the fibres has been obtained from fracture surfaces. This has revealed that the fibrous structures are manganese-sulphide

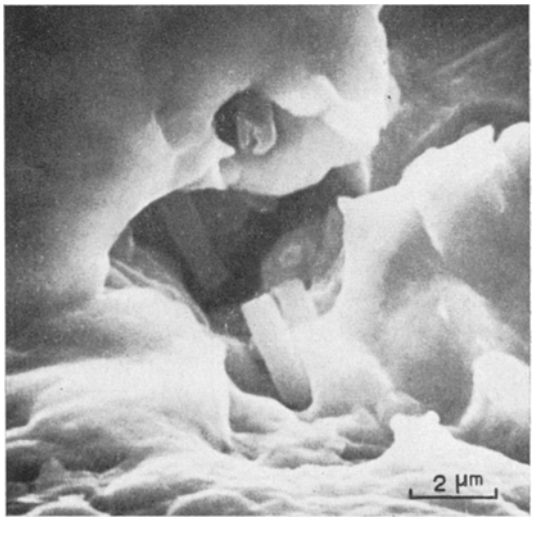

Figure 24 MnS inclusions at the centre the specimen aligned perpendicular to the specimen surface.

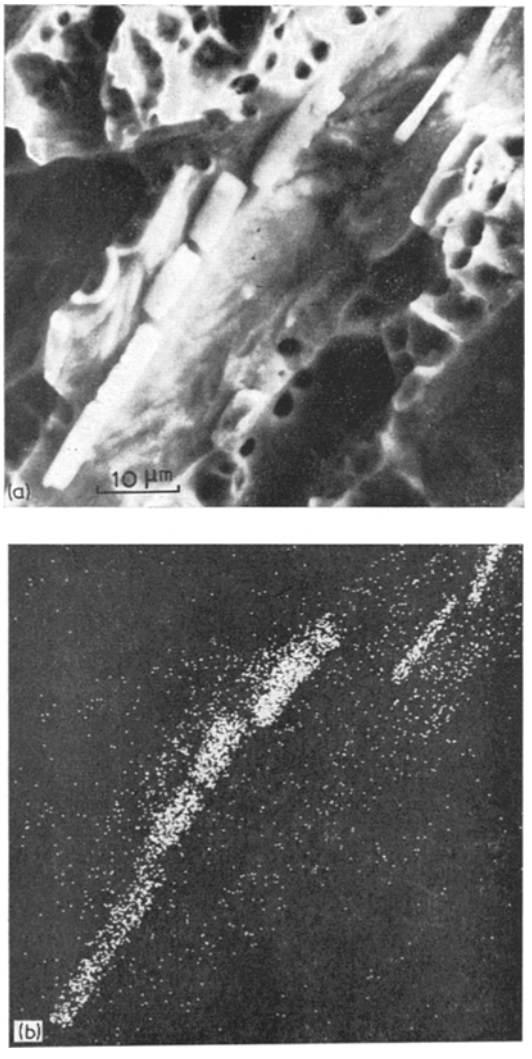

Figure 25 (a) Secondary electron image of different diameter fibres. (b) S$K\alpha$ X-ray image of (a).

inclusions. Fig. 25b illustrates the characteristic X-ray image of S$K\alpha$ of the fibres in Fig. 25a. This micrograph shows that there is no composition difference between different diameter fibres.

It is known that sputter yields increase fairly steadily within each group of elements reaching a maximum for the inert gas species of the group [2]. Since the yield falls almost to zero thereafter, reference to the work of Laegreid and Wehner [35] implies that the sputter yield of sulphur is very low. Wehner [36] has shown that the sputter yield of steel is obtained solely by taking the average of the sum of the yields of the constituent elements. Thus, in the present case, the sulphide component of the fibre must drastically reduce the total yield of the inclusion, and this would explain the taller fibre protrusions compared to the shorter cones. The slowness of the fibre erosion also accounts for the predominance of dome type ends mentioned earlier. The presence of such MnS fibres is not unexpected since manganese is an additive to the ladle to deoxidize the steel. In addition, manganese takes up sulphur from the matrix in order to neutralize injurious effects such as cracking that sulphur would otherwise have upon the hot-rolling properties of the steel.

5. Discussion

The formation of cones and rods can be understood from the theories of Stewart and Thompson [16], Carter *et al* [26-28] and Barber *et al* [7] and this will be discussed below. It must be emphasized, however, that all these theories only treat surface changes in terms of atomic ejections and thus they neglect surface diffusion processes, localized surface binding energy variations and redeposition of sputtered material.

In the present investigation, the cones have been shown to originate from non-metallic inclusions. Such particles, being of different composition and hence sputter yield from the bulk, will shield the underlying matrix material. Protrusions can thus develop on the bombarded surface as the matrix is preferentially etched away. In considering cone formation, two simultaneous processes must be taken into account. These are the ion etching of the second phase particles and the ion bombardment of the matrix material.

The sputter yield curve has a form which typically increases with a sec θ dependence from a value $S(0)$ at $\theta = 0°$. A maximum occurs at $\theta = \pm\hat{\theta}$ after which the yield falls to zero at $\theta = \pm 90°$. Carter *et al* [26, 27] show that the only stable configuration allowing progression of the surface in a direction parallel to the beam occurs when planar surfaces are at an angle θ to the ion beam such that $\theta = \pm 90°$, a vertical surface, $\theta = 0°$, a horizontal surface, and $\theta = \pm\hat{\theta}$, a plane inclined at $\hat{\theta}$ to the horizontal. Surfaces with other inclinations to the ion-bombardment direction will thus change to one of these slopes.

In general, a precipitate or contaminant particle such as dust will have curvature on at least part of its surface. Unless the tangent to the

surface makes one of the above angles to the beam a change in curvature will result with ion etching. The structure will subsequently pass though a series of intermediate shapes. The element of curvature which corresponds to greatest sputter yield will finally predominate so that all curves become planes terminating in one of the above orientations. Thus, it can be seen that with increasing ion-etching time, a hillock develops on the surface. The sputter yield difference between the particle and the matrix will cause this structure to increase in size while simultaneously the surface curvatures change until, if p and m denote particle and matrix, slopes of $\theta = \pm(\hat{\theta})_p$ develop. These slopes are then the generator of a metastable cone structure of semi-vertical angle $90° - (\hat{\theta})_p$. If this shape does not develop uniformly round the particle due to the particle topography, an asymmetric cone with respect to the axis, the ion beam direction, will result, see Fig. 22. In general, however, all things average out and symmetry prevails.

A cone structure of the above given cone apex angle will always develop from a lower yield inclusion unless the inclusions dimensions are such that it is eroded away before this process is complete. This characteristic cone apex angle is found to be a function of the atomic numbers of the ion and target atoms, crystal structure of the target material, and ion energy. Calculations concerning the prediction of cone angles will be published shortly [25].

Even when a cone finally develops on the surface, this is not an equilibrium condition since although the plane at $(\hat{\theta})_p$ alone remains constant in orientation, it does have a velocity parallel to the ion-beam direction. Three possibilities then exist.

(1) If $S(\hat{\theta})_p < S(0)_m$ the developing protrusion can increase in height with bombardment time, until the inclusion is etched away. The matrix cone will then rapidly decrease in size and finally disappear.

(2) When $S(\hat{\theta})_p = S(0)_m$, the cone and matrix remain in step until the inclusion is eroded away.

(3) For $S(\hat{\theta})_p > S(0)_m$, the particle is sputtered away faster than the matrix material with the result that the cone quickly decreases in size and subsequently vanishes.

As emphasized by Nobes *et al* [26], micro-cone development will only continue until the contaminant, defect or precipitate is eventually sputtered away. At that stage, the situation will be again unstable, since except in the region close to $\theta = 90°$, $S(\hat{\theta})_m > S(0)_m$ and the matrix conical protrusion of semi-vertical angle $90° - (\hat{\theta})_m$ can only erode in the direction of the ion beam at a rate faster than the surrounding surface plane. True equilibrium can thus only occur when the cone of matrix material is finally planed down.

The above argument applies to cones as well as pillars. In the latter case, the only difference is the dimensions and composition. The pillars will thus have a different sputter yield from the cones due to composition and this will affect the rate at which changes occur and structure development proceeds.

Acknowledgements

The author is indebted to the Ministry of Technology, now Department of Trade and Industry, UK for financial support during the preparation of an initial number of specimens. All the subsequent work has been carried out in collaboration with the Solid State Physics Research Unit at the University of the Witwatersrand and sponsorship by the CSIR, South Africa, is gratefully acknowledged. For aid with particle analysis, sincere thanks is extended to Mr P. Ellis at the National Research Institute for Occupational Diseases, Johannesburg for his help on EMMA-4, and to Dr J. Smuts at the South African Iron and Steel Industrial Corporation Limited, Pretoria, for operating the JXA-5A microprobe. Appreciation is expressed to Dr D. J. Barber for a copy of his paper prior to publication. Helpful discussions with Dr D. Dew-Hughes, Mr C. E. Mavrocordatos and Mr R. Rickard are gratefully acknowledged.

References

1. M. KAMINSKY, "Atomic and Ionic Impact Phenomena on Metal Surfaces" (Springer-Verlag, Berlin, 1965).
2. G. CARTER and J. S. COLLIGON, "Ion Bombardment of Solids" (Heinemann, London, 1968).
3. W. R. GROVE, *Phil. Trans. Roy. Soc.* **142** (1852) 87.
4. D. M. MCCUTCHEN, *J. Appl. Phys.* **20** (1949) 414.
5. D. M. MCCUTCHEN and W. PAHL, *Met. Progr.* **56** (1949) 674.
6. P. R. THORNTON, "Scanning Electron Microscopy" (Chapman and Hall, London, 1968) p. 305.
7. D. J. BARBER, F. C. FRANK, M. MOSS, J. W. STEEDS and I. S. T. TSONG, *J. Mater. Sci.* **8** (1973) 1030.
8. H. FETZ, *Z. Phys.* **119** (1942) 590.
9. A. GÜNTHERSCHÜLZE and W. TOLLMEIN, *ibid* **119** (1942) 685.

10. G. V. SPIVAK, I. N. PRILEZHAEVA and O. I. SAVOCHKINA, *Dokl. Acad. Nauk. SSR* **88** (1953) 511.
11. G. K. WEHNER, *J. Appl. Phys.* **26** (1955) 1056.
12. A. D. G. STEWART, Proc. 5th Int. Conf. on Electron Microscopy, Philadelphia, 1962 (Academic Press, New York, 1962) D.12.
13. A. D. G. STEWART, see W. C. NIXON, *Contemporary Physics* **10** (1969) 71.
14. R. F. W. PEASE, A. N. BROERS and R. A. PLOC, Proc. 3rd Eur. Conf. on Electron Microscopy, Prague, 1964 (Czechoslovak Acad, of Sci., Prague, 1965) Vol. A, p. 389.
15. V. MARINKOVIC and B. NAVINSEK, *ibid* p. 311.
16. A. D. G. STEWART and M. W. THOMPSON, *J. Mater. Sci.* **4** (1969) 56.
17. I. H. WILSON and M. W. KIDD, *ibid* **6** (1971) 1362.
18. M. J. WITCOMB, Proc. of the Southern African Electron Microscopy Society, Johannesburg (1972) p. 75.
19. G. K. WEHNER and D. J. HAJICEK, *J. Appl. Phys.* **42** (1971) 1145.
20. M. W. THOMPSON, *Phil. Mag.* **18** (1968) 377.
21. G. K. WEHNER, *Phys. Rev.* **102** (1956) 690.
22. G. S. ANDERSON and G. K. WEHNER, *J. Appl. Phys.* **31** (1960) 2305.
23. R. S. NELSON and M. W. THOMPSON, *Proc. Roy. Soc.* (Lond.) **A259** (1961) 458.
24. D. J. MAZEY, R. S. NELSON and P. A. THACKERY, *J. Mater. Sci.* **3** (1968) 26.
25. M. J. WITCOMB, to be published.
26. M. J. NOBES, J. S. COLLIGON and G. CARTER, *J. Mater. Sci.* **4** (1969) 730.
27. G. CARTER, J. S. COLLIGON and M. J. NOBES, *ibid* **6** (1971) 115.
28. C. CATANA, J. S. COLLIGON and G. CARTER, *ibid* **7** (1972) 467.
29. H. KOENIG and G. HELWIG, *Z. Phys.* **129** (1951) 491.
30. R. C. BRADLEY, *J. Appl. Phys.* **30** (1959) 1.
31. R. L. CUNNINGHAM and J. NG-YELIM, *ibid* **40** (1969) 2904.
32. R. KIESSLING and N. LANGE, "Non-metallic Inclusions in Steel", Part 1, Special Report 90 (Iron and Steel Institute, London, 1964) p. 48.
33. H. J. GOLDSCHMIDT, "Interstitial Alloys" (Butterworths, London, 1967) p. 592.
34. A. R. BAYLY and P. D. TOWNSEND, Atomic Collisions in Solids group meeting, Polytechnic, South Bank (2 June 1971).
35. N. LAEGREID and G. K. WEHNER, *J. Appl. Phys.* **32** (1961) 365.
36. G. K. WEHNER, *ibid* **112** (1958) 1120.

Received 19 September and accepted 16 October 1973.